

Microstructure, Mechanical Properties and Fracture Behavior of As-Extruded Zn–Mg Binary Alloys

Li-Qing Wang¹ · Yu-Ping Ren¹ · Shi-Neng Sun¹ · Hong Zhao¹ · Song Li¹ · Gao-Wu Qin¹

Received: 11 January 2017/Revised: 27 February 2017/Published online: 26 April 2017
© The Chinese Society for Metals and Springer-Verlag Berlin Heidelberg 2017

Abstract In the present work, Zn–(0–1)Mg (wt%) alloys were prepared by casting and indirect extrusion at 200 and 300 °C, respectively. With Mg addition, both the size and amount of second phase Mg₂Zn₁₁ increased, and the equiaxed grains were significantly refined. The extrusion temperature had little influence on Mg₂Zn₁₁, but the grains were refined at low extrusion temperature. For the alloys extruded at 200 °C, as Mg content increased, the tensile yield strength (TYS) increased from 64 MPa for pure Zn to 262 MPa for Zn–1Mg; the elongation increased from 14.3% for pure Zn to 25% for Zn–0.02Mg and then decreased to 5% for Zn–1Mg. For the alloys extruded at 300 °C, as Mg content increased, the TYS increased from 67 MPa for pure Zn to 252 MPa for Zn–1Mg, while the elongation decreased from 11.7% to 2%. The alloy extruded at 200 °C exhibited higher TYS and elongation than the corresponding alloy extruded at 300 °C. The combination of grain refinement and second phase Mg₂Zn₁₁ contributed to the improvement in the TYS, and the grain refinement played a major role in strengthening alloy. Zn–0.02Mg and Zn–0.05Mg alloys extruded at 200 °C show a mixture of cleavage and ductile fracture corresponding to higher elongation, while the other alloys show cleavage fracture.

KEY WORDS: Zn–Mg binary alloy; Indirect extrusion; Microstructure; Mechanical property; Fracture behavior

1 Introduction

Zinc (Zn) is an essential trace element and plays important roles in various aspects of basic biological function in human body [1, 2]. Besides, Zn with a standard electrode potential of –0.8 V is between that of Mg (–2.4 V) and Fe (–0.4 V) [3, 4], which provides its moderate degradability.

As Zn has a low melting point of 420 °C and low reactivity in molten state, it favors an easy manufacture. Therefore, it has attracted much attention to develop new biodegradable Zn-based materials in recent years. Bowen et al. [5] implanted pure Zn wires into the abdominal aorta of adult male Sprague–Dawley rats. It indicated that the in vivo degradation rate increased linearly from 10 to 50 μm/year within 6 months. Vojtech et al. [6] studied the in vitro degradation rates of the as-cast Zn–(0–3)Mg alloys (wt%, all of the contents refer to weight percentage if not specifically stated). The results showed that the degradation rates of Zn–Mg alloys were much lower than those of Mg alloys, indicating that Zn-based alloys could be potential candidates for biodegradable material.

However, pure Zn and the as-cast Zn–Mg alloys were difficult to satisfy the mechanical properties requirement of the implant materials. Recently, new binary and ternary Zn-based alloys containing Mg, Ca, Sr and Mn were

Available online at <http://link.springer.com/journal/40195>.

✉ Yu-Ping Ren
renyp@atm.neu.edu.cn

✉ Gao-Wu Qin
qingw@smm.neu.edu.cn

¹ Key Laboratory for Anisotropy and Texture of Materials (Ministry of Education), School of Materials Science and Engineering, Northeastern University, Shenyang 110819, China

achieved by hot extrusion and rolling [3, 6–14]. These Zn-based alloys exhibited good biocompatibility, appropriate degradation rate and significantly improved mechanical properties. Till now, most of the work focused on the biocompatibility, while the influence of the microstructure on the mechanical properties of the Zn-based alloys has rarely been studied. The mechanical properties of pure Zn are strongly dependent on the extrusion process. The tensile yield strength (TYS), ultimate tensile strength (UTS) and elongation reached 35 MPa, 65 MPa and 4% for pure Zn extruded at 210 °C [12, 13], 55 MPa, 100 MPa and 7.5% for pure Zn extruded at 300 °C [7], and 130 MPa, 180 MPa and 54% for pure Zn extruded at 200 °C [11]. The reasons for such large differences in mechanical properties are not clearly stated and might be ascribed to grain size and texture caused by the different extrusion processes. Furthermore, the Zn–0.8Mg alloy [7] extruded at 300 °C showed TYS, UTS and elongation of 203 MPa, 301 MPa and 15%, respectively. The microstructure analysis showed that it was composed of Mg_2Zn_{11} , $MgZn_2$ and equiaxed grains with a size of 12 μm , while the TYS and UTS of Zn–1.6Mg alloy [7] were higher, but the elongation significantly decreased to about 4% due to the only second phase Mg_2Zn_{11} distributed as continuous network. Gong *et al.* [11] reported that the Zn–1Mg alloy extruded at 200 °C exhibited TYS, UTS and elongation of 180 MPa, 250 MPa and 12%, respectively. The as-extruded Zn–1Mg alloy contained the grains with size of 5 μm and fine precipitates segregated along grain boundaries. So the low extrusion temperature was beneficial to grain refinement, and precipitation of the second phase played important role in improving mechanical properties. Li *et al.* [12, 13] prepared Zn–1X and Zn–1X–1Y (X, Y = Mg, Ca, Sr) alloys by hot rolling and hot extrusion. The TYS, UTS and elongation of the Zn-based alloys were between 140–220 MPa, 200–260 MPa and 5–20%, respectively. The binary and ternary Zn-based alloys contained one or two kinds of second phases among $MgZn_2$, $CaZn_{13}$ and $SrZn_{13}$. The as-rolled Zn–1Mg–0.1Mn alloy [8] containing the only second phase $MgZn_2$ exhibited TYS, UTS and elongation values of 195 MPa, 300 MPa and 26%, respectively, while the as-rolled Zn–1Mg–0.1Sr alloy [9] containing second phases $MgZn_2$ and $SrZn_{13}$ exhibited TYS, UTS and elongation values of 197 MPa, 300 MPa and 22%. However, the mechanical properties of the Zn-based alloys have not been well understood due to the lack of the microstructural characterization.

Therefore, for the Zn–Mg-based alloys, both the alloying element content and manufacturing history had influence on the microstructures, in turn, the mechanical properties. In the present work, Zn–(0–1)Mg alloys were selected according to Zn–Mg phase diagram [15] for extrusion at 200 and 300 °C, respectively. The microstructure, mechanical properties and

fracture behavior of the as-extruded Zn–Mg alloys were studied, and it will provide reference for designing and preparation of biodegradable Zn-based alloys.

2 Materials and Methods

Pure Zn and Zn–(0.02–1)Mg binary alloys were prepared by melting pure Zn (99.95 wt%) and Mg (99.95 wt%) in a resistance furnace in air. The melting temperature did not exceed 500 °C for preventing excessive evaporation of the volatile zinc. Cylindrical ingots (Φ 60 mm) were obtained by casting into a non-preheated steel mold. After the homogenization treatment at 330 °C for 4 h, the ingots were machined to billets for extrusion (Φ 48 \times 100 mm). Then, the indirect extrusion was carried out at 200 and 300 °C, respectively, with an extrusion ratio of 16:1, ram speed of about 3 mm/s. The cylindrical rods of 12 mm in diameter were obtained. Finally the extruded rods were cooled in air. The actual composition of the investigated Zn–Mg binary alloys was determined by an inductively coupled plasma atomic emission spectrometer (ICP-AES, Optima 4300DV, PE, USA), which is given in Table 1.

The microstructure of the as-extruded alloys was investigated by optical microscopy (OM) (OLYMPUS GX-71), scanning electron microscopy (SEM) (JEOL JSM-6510A) and X-ray diffraction (XRD) (Philips PW3040/60). Samples parallel to the extrusion direction were taken from the extrudate. They were ground up to 2000 grit by SiC paper, followed by mechanically polishing with 0.5 μm diamond pastes. Samples for OM were etched for 3–10 s in a solution of 10% hydrochloric acid and 90% alcohol and then washed immediately using alcohol. Grain size was measured using the linear intercept method on the OM images. The second phase was analyzed by XRD with $Cu-K\alpha$ radiation and scan rate of 3°/min.

Mechanical properties were characterized by tensile test. Tensile specimens with 5 mm in diameter and gauge length of 25 mm were machined from the extruded rods. The tensile test was carried out at a constant cross-head speed of 1.5 mm/min at room temperature. Three samples were tested for each alloy. Then, TYS, UTS and elongation of all

Table 1 Mg content of the as-extruded Zn–Mg binary alloys (wt%)

Alloys	Mg
Zn–0.02Mg	0.024
Zn–0.05Mg	0.056
Zn–0.2Mg	0.216
Zn–0.5Mg	0.464
Zn–1Mg	0.975

the alloys were determined. The fracture surface after tensile tests was observed by SEM.

3 Results

3.1 Microstructure

Figure 1 shows the optical micrographs of Zn–(0–1)Mg alloys extruded at 200 and 300 °C. The as-extruded Zn–Mg alloys exhibited equiaxed grains, and the twins were observed in the as-extruded Zn–(0–1)Mg alloys. During the hot extrusion process, the Zn matrix experienced fully dynamic recrystallization, and the grain size significantly decreased with increasing Mg content, as shown in Fig. 2. As Mg content increased from 0 to 0.2 wt%, the grain size decreased from 112 to 16 µm after the alloys were extruded at 200 °C, and the grain size decreased from 203 to 38 µm after extruded at 300 °C. It is apparent that the grain size of the alloys extruded at 200 °C was about half of that of the alloys extruded at 300 °C, meaning that the lower extrusion temperature favored the grain refinement of the Zn–(0–0.2)Mg alloys. However, for Zn–0.5Mg and Zn–1Mg, the grain size kept at about 10 µm, and the extrusion temperature had little influence on the grain size.

The back-scattered electron (SEM-BSE) images of the as-extruded Zn–(0.02–1)Mg alloys are shown in Fig. 3. Evidently only one kind of second phase was found in these alloys. Meanwhile, the XRD patterns of Zn–1Mg extruded at 200 and 300 °C confirmed that the second phase was Mg₂Zn₁₁ as shown in Fig. 4. The amount and size of Mg₂Zn₁₁ increased with an increase in Mg content and showed little difference in the alloy extruded at different temperatures. Mg₂Zn₁₁ particles formed in Zn–0.02Mg with an average size of 0.5 µm and reached between 0.4 and 2 µm in size corresponding to the average size of 0.8 µm in Zn–0.05Mg. When Mg content was more than 0.2 wt%, Mg₂Zn₁₁ distributed along the grain boundaries as shown in Fig. 1 and gradually transformed into strip shaped and distributed parallel to the extrusion direction. In Zn–1Mg alloy, the length of the strip Mg₂Zn₁₁ elongated to 20 µm which was larger than the matrix grain size, and also some small Mg₂Zn₁₁ particles about 1 µm in size were observed.

3.2 Mechanical Properties

Figure 5a, b shows the room temperature engineering stress–strain curves of the Zn–Mg alloys extruded at 200 and 300 °C, respectively. For Zn–0.02Mg extruded at 200 °C and Zn–0.02Mg and Zn–0.05Mg extruded at 300 °C, obvious serrated flow behavior on the curves occurred after yielding of the alloys. This phenomenon was

related to the nucleation of deformation twins during tensile process [16].

The mechanical properties including TYS, UTS and elongation are summarized in Fig. 5c, d. Firstly, both the TYS and UTS continuously increased as Mg content increased. After the extrusion at 200 °C, TYS and UTS were 64 and 110 MPa for pure Zn and were improved to 262 and 330 MPa for Zn–1Mg, while extruded at 300 °C, TYS and UTS were 67 and 109 MPa for pure Zn and were also improved to 253 and 323 MPa for Zn–1Mg. The TYS and UTS of pure Zn showed less independence on the extrusion temperatures. However, Zn–(0.02–1)Mg alloys extruded at 200 °C possessed higher TYS and UTS than Zn–(0.02–1)Mg alloys extruded at 300 °C. Therefore, according to the variations of the microstructures mentioned above, the strength of the as-extruded Zn–Mg alloys is generally dominated by the combinations of solid solution strengthening, grain refinement and precipitation strengthening. Secondly, after the extrusion at 200 °C, the elongation increased from 14.3% for pure Zn to 25% for Zn–0.02Mg, then decreased when Mg content exceeded 0.02 wt% and finally reached about 5% for Zn–1Mg. But the elongation of Zn–(0–1)Mg alloys extruded at 300 °C showed different trend, and it continuously decreased from 11.7% to about 2% as Mg content increased. Meanwhile, it showed that Zn–(0–1)Mg alloys extruded at 200 °C exhibited improved ductility compared with the same alloy extruded at 300 °C.

3.3 Fracture Behavior

To verify the fracture mechanisms and their relations with the mechanical properties, the fracture surface was observed and is shown in Figs. 6 and 7. It is seen that Zn–0.02Mg and Zn–0.05Mg extruded at 200 °C exhibited quite different morphologies from the other alloys. Except Zn–0.02Mg and Zn–0.05Mg extruded at 200 °C, the other Zn alloys showed characteristic of brittle fracture. It could be observed intragranular cracks, cleavage steps and cleavage planes surrounded by tearing ridges in pure Zn, which indicated typical cleavage fracture mode. But as Mg content increased, the size of cleavage planes decreased. Meanwhile, with increasing Mg₂Zn₁₁ amount and size, the fracture between the Zn matrix and Mg₂Zn₁₁ happened more frequently, and the area of tearing ridges reduced and even disappeared, which resulted in the gradual reduction in elongation.

The fracture surface of Zn–0.02Mg and Zn–0.05Mg extruded at 200 °C is shown in Fig. 6c, e and d, f, respectively. It could be observed obvious tear lip in morphology at low magnification. However, at high magnification, the fractures consisted of cleavage planes, tearing ridges and some dimples. It meant that both alloys showed a mixture of cleavage and ductile fracture modes

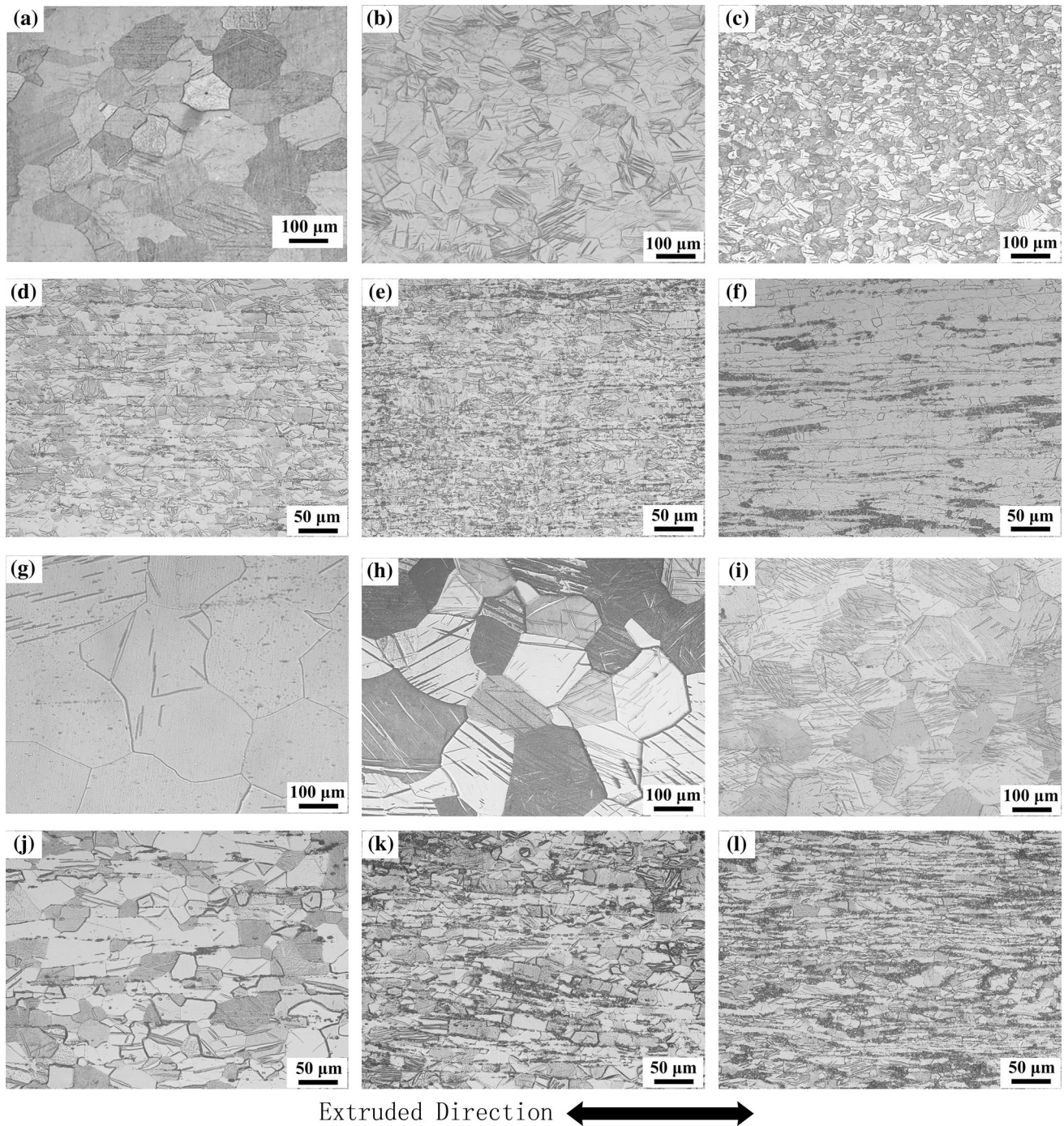


Fig. 1 Optical micrographs of the Zn–Mg binary alloys on longitudinal section: **a** pure Zn at 200 °C, **b** Zn–0.02Mg at 200 °C, **c** Zn–0.05Mg at 200 °C, **d** Zn–0.2Mg at 200 °C, **e** Zn–0.5Mg at 200 °C, **f** Zn–1Mg at 200 °C, **g** pure Zn at 300 °C, **h** Zn–0.02Mg at 300 °C, **i** Zn–0.05Mg at 300 °C, **j** Zn–0.2Mg at 300 °C, **k** Zn–0.5Mg at 300 °C, **l** Zn–1Mg at 300 °C

and corresponded to larger elongation of 25 and 13.6%, respectively. The ductile fracture was determined by the size of the dimples which were originated from microvoids aggregation, while the formation of the microvoids and resultant dimples were attributed to fracture of Mg_2Zn_{11} particles and Zn matrix. On the other hand, when

comparing the other Zn alloys with Zn–0.02Mg or Zn–0.05Mg extruded at 200 °C containing similar Mg_2Zn_{11} particles or grain size, the brittle cleavage fracture to ductile fracture transition was in relation to proper matching of the size and volume fraction of Mg_2Zn_{11} particle and grain size.

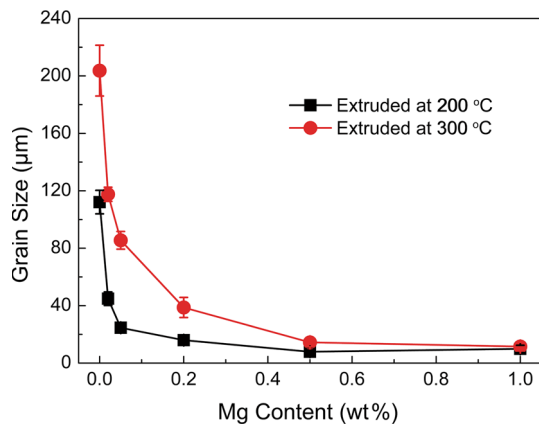


Fig. 2 Variation of the average grain size of the Zn–Mg binary alloys with Mg content

4 Discussion

4.1 Microstructure

In the present work, the Zn–(0–1)Mg alloys were prepared by indirect extrusion at 200 and 300 °C. During the hot extrusion process, Mg_2Zn_{11} compound was broken up and arranged along the extrusion direction; meanwhile, the equiaxed grains of Zn matrix formed during dynamic recrystallization. The size of the recrystallized grains was primarily influenced by extrusion temperature and hinderance of Mg_2Zn_{11} , finally leading to the variation of grain sizes in Fig. 2. For pure Zn, the grain size was reduced by 50% as the extrusion temperature decreased from 300 to 200 °C. Usually lower extrusion temperature reduced the grain boundary migration rate [17] and finally resulted in the grain refinement. For Zn–(0.02–1)Mg alloys, except for the effect of extrusion temperature, Mg_2Zn_{11} particles played an important role in the grain refinement by not only serving as the crystal nucleus to facilitate the nucleation of recrystallization, but also pinning grain boundary to retard the grain growth. The effect of the particles on the grain refinement can be expressed by Zener pinning pressure (P_Z) [17, 18]:

$$P_Z = \frac{3f_s\gamma}{2r}, \quad (1)$$

where f_s and r are the second phase volume fraction and radius, respectively, and γ is grain boundary interfacial energy. It means that alloy with greater P_Z would exhibit smaller grain size. In the present work, as Mg content increased from 0 to 0.2 wt%, the increase in f_s was greater than that in r , and it resulted in the increase in P_Z . So the grain size decreased significantly with Mg addition. On the other hand, the grain sizes of Zn–(0.02–0.2)Mg alloys extruded at 200 °C were less than half of those extruded at

300 °C, which meant that the extrusion temperature still had obvious effect on the grain refinement. However, when Mg content reached 0.5 and 1 wt%, the increase in f_s was almost equal to the increase in r . So the grain size of these alloys was not further refined and kept at about 10 μm. Besides, the extrusion temperature had very slightly influence on the grain refinement for Zn–0.5Mg and Zn–1Mg. Furthermore, according to Eq. (1), the grain size still was potential further to refined by reducing the size of Mg_2Zn_{11} , especially for Zn–0.5Mg and Zn–1Mg.

4.2 Mechanical properties

As for the relationship between the microstructure and mechanical properties of the as-extruded Zn–(0–1)Mg alloys, the strengthening mechanism models for TYS can be divided into solid solution strengthening, $\Delta\sigma_{SS}$; grain boundary strengthening, $\Delta\sigma_g$; and second phase strengthening, $\Delta\sigma_S$. Therefore, TYS (σ_y) of the Zn–Mg alloys can be approximated as:

$$\sigma_y = \sigma_0 + \Delta\sigma_{SS} + \Delta\sigma_g + \Delta\sigma_S, \quad (2)$$

where σ_0 is the intrinsic resistance of the lattice to dislocation motion. Each of the strengthening mechanisms for the Zn–Mg alloys is discussed as follows.

(1) Solid solution strengthening depends on the solute concentration of Mg in Zn matrix and can be expressed as:

$$\Delta\sigma_{SS} = k \times c^n, \quad (3)$$

where k is the strengthening constant in solute, c is the atomic concentration of solute, n is a constant and usually taken as 1/2 or 2/3 [19–21]. Liu *et al.* [22] pointed out that the contribution of solid solution strengthening for 0.03 wt% Mg dissolved in Zn matrix was about 12 MPa. However, in the present Zn–(0–1)Mg alloys, Mg_2Zn_{11} particles precipitated in Zn–0.02Mg, and both the volume fraction and size of Mg_2Zn_{11} increased with increasing Mg content. Therefore, the concentration of Mg dissolved in Zn matrix could not exceed 0.02 wt% (i.e., 0.0054 at.%). So it is regarded that the contribution of solid solution strengthening to TYS could be neglected.

(2) The grain boundary strengthening is calculated according to Hall–Petch relationship [19–21] as follows:

$$\Delta\sigma_g = k_{H-P} \times d_g^{-1/2}, \quad (4)$$

where k_{H-P} is the Hall–Petch constant and d_g is the grain size. In the present work, $\sigma_0 = 32.3$ MPa and $k_{H-P} = 220$ MPa $\mu m^{1/2}$ [23] were adopted for pure Zn, while $\sigma_0 = 11$ MPa and $k_{H-P} = 580$ MPa $\mu m^{1/2}$ [22] were adopted for Zn–(0.02–1)Mg alloys. The contributions of grain boundary strengthening to TYS of the as-extruded Zn–(0–1)Mg alloys are listed in Tables 2 and 3.

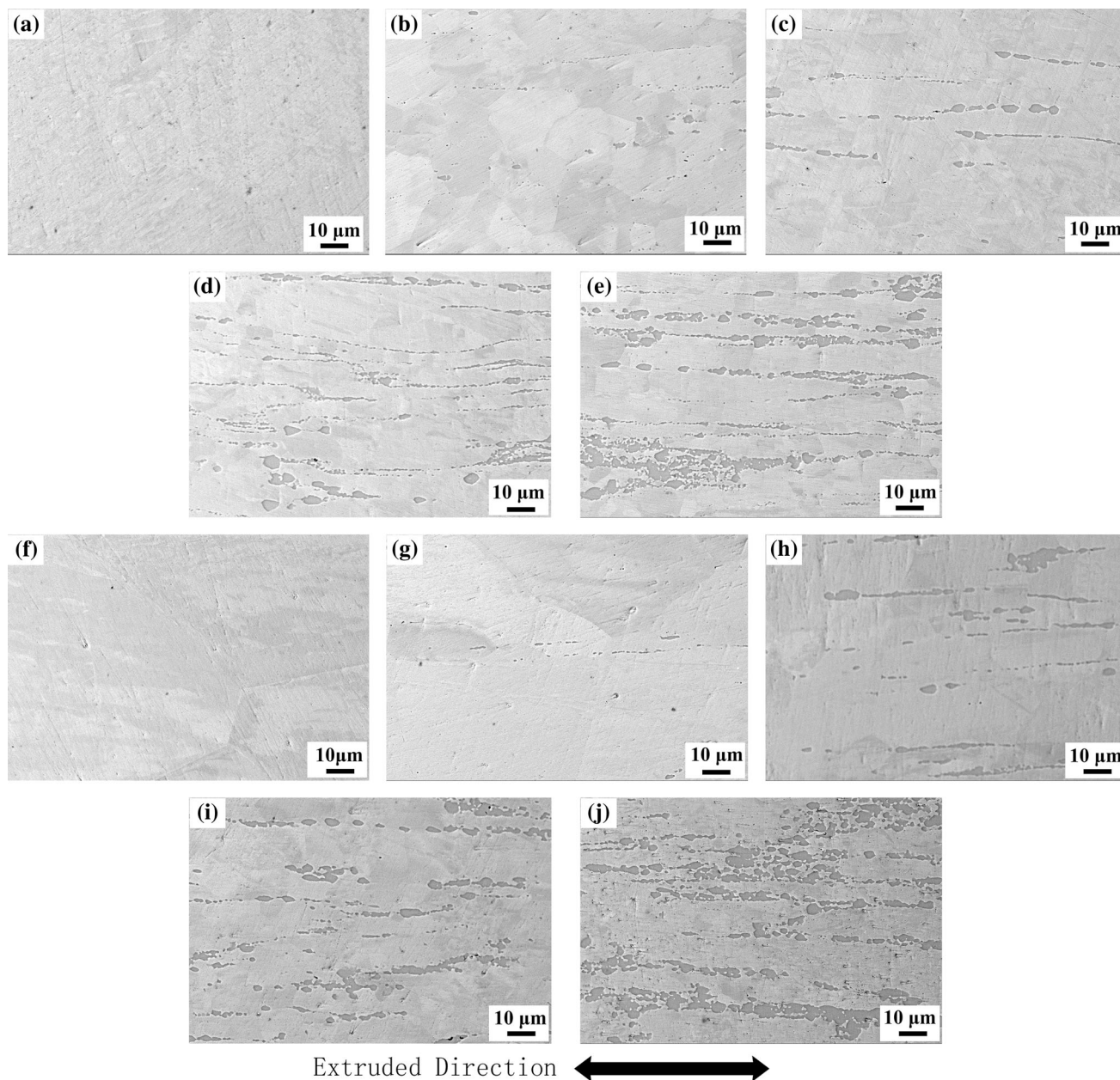


Fig. 3 SEM-BSE morphologies of the Zn–Mg binary alloys on longitudinal section: **a** Zn–0.02Mg at 200 °C, **b** Zn–0.05Mg at 200 °C, **c** Zn–0.2Mg at 200 °C, **d** Zn–0.5Mg at 200 °C, **e** Zn–1Mg at 200 °C, **f** Zn–0.02Mg at 300 °C, **g** Zn–0.05Mg at 300 °C, **h** Zn–0.2Mg at 300 °C, **i** Zn–0.5Mg at 300 °C, **j** Zn–1Mg at 300 °C

(3) Second phase strengthening originates from the different properties between the second phase and matrix and depends on the morphology, volume fraction and size of second phase. In the present work, Zn–0.02Mg and Zn–0.05Mg alloys contained small $\text{Mg}_2\text{Zn}_{11}$ particles distributing along the grain boundaries. Thus, the strengthening mechanism can be classified into load transfer from Zn matrix to $\text{Mg}_2\text{Zn}_{11}$, $\Delta\sigma_{\text{LT}}$; dislocation generation due to the difference in thermal expansion between Zn matrix and $\text{Mg}_2\text{Zn}_{11}$, $\Delta\sigma_{\text{CTE}}$; and dislocation–particle interaction by

Orowan process, $\Delta\sigma_{\text{OR}}$ [19, 24]. Then, second phase strengthening can be expressed in the following equation:

$$\begin{aligned} \Delta\sigma_{\text{S}} &= \Delta\sigma_{\text{LT}} + \Delta\sigma_{\text{CTE}} + \Delta\sigma_{\text{OR}} \\ &= \frac{1}{2}\sigma_{\text{M}}f_{\text{S}} + \alpha Gb \left(\frac{12 \cdot \Delta T \cdot \Delta C \cdot f_{\text{S}}}{b \cdot d_{\text{S}}} \right)^{1/2} \\ &\quad + M \frac{0.81Gb}{2\pi\sqrt{1-\nu}} \left(0.615d_{\text{S}}\sqrt{\frac{2\pi}{3f_{\text{S}}}} - d_{\text{S}} \right)^{-1} \ln \frac{d_{\text{S}}}{b}, \end{aligned} \quad (5)$$

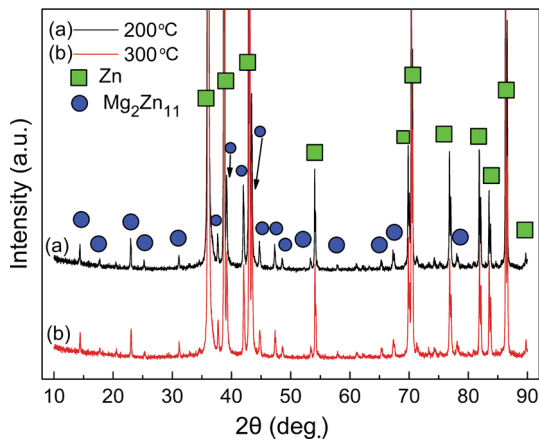


Fig. 4 X-ray diffraction patterns of the Zn–1Mg alloys extruded at 200 and 300 °C

where σ_M is the TYS of Zn matrix, f_S is the volume fraction of Mg_2Zn_{11} particles, α is a constant taken as 1, G is the shear modulus of Zn matrix ($=43$ GPa), b is the Burgers vector ($=0.2664$ nm), ΔT is the temperature change between the extrusion and tensile testing, ΔC is the difference in thermal expansion coefficient between Zn

($C_{Zn} = 30.2 \times 10^{-6} K^{-1}$) and Mg_2Zn_{11} ($C_{Mg_2Zn_{11}}$ has not been obtained), so $\Delta C = 0-30.2 \times 10^{-6} K^{-1}$, d_S is the mean diameter of Mg_2Zn_{11} , M is the Taylor factor ($=6.5$ [19, 23]), ν is the Poisson’s ratio ($=0.25$).

When Mg content reached 0.2, 0.5 and 1 wt%, the size of Mg_2Zn_{11} obviously increased; moreover, it was also larger than that of Zn grains. So the strengthening effect by interaction between dislocations and particles was no longer adapted. In this case, the discontinuous strip-shaped Mg_2Zn_{11} would act as discontinuous fibers to undertake load. Therefore, the law of mixtures in discontinuous fiber composite materials can be introduced to these Zn–Mg alloys and given as [25]:

$$\sigma_y = \sigma_M(1 - f_S) + \lambda\sigma_S f_S, \tag{6}$$

where σ_y is TYS of Zn–Mg alloy, σ_S is TYS of Mg_2Zn_{11} , λ is correction coefficient and can be expressed as:

$$\lambda = \frac{L}{2l_c}, \tag{7}$$

where L is the length of Mg_2Zn_{11} , l_c is the critical length of Mg_2Zn_{11} : when $L > l_c$, the invalidation of Zn–Mg alloy is caused by the fracture of Mg_2Zn_{11} ; when $L < l_c$, the

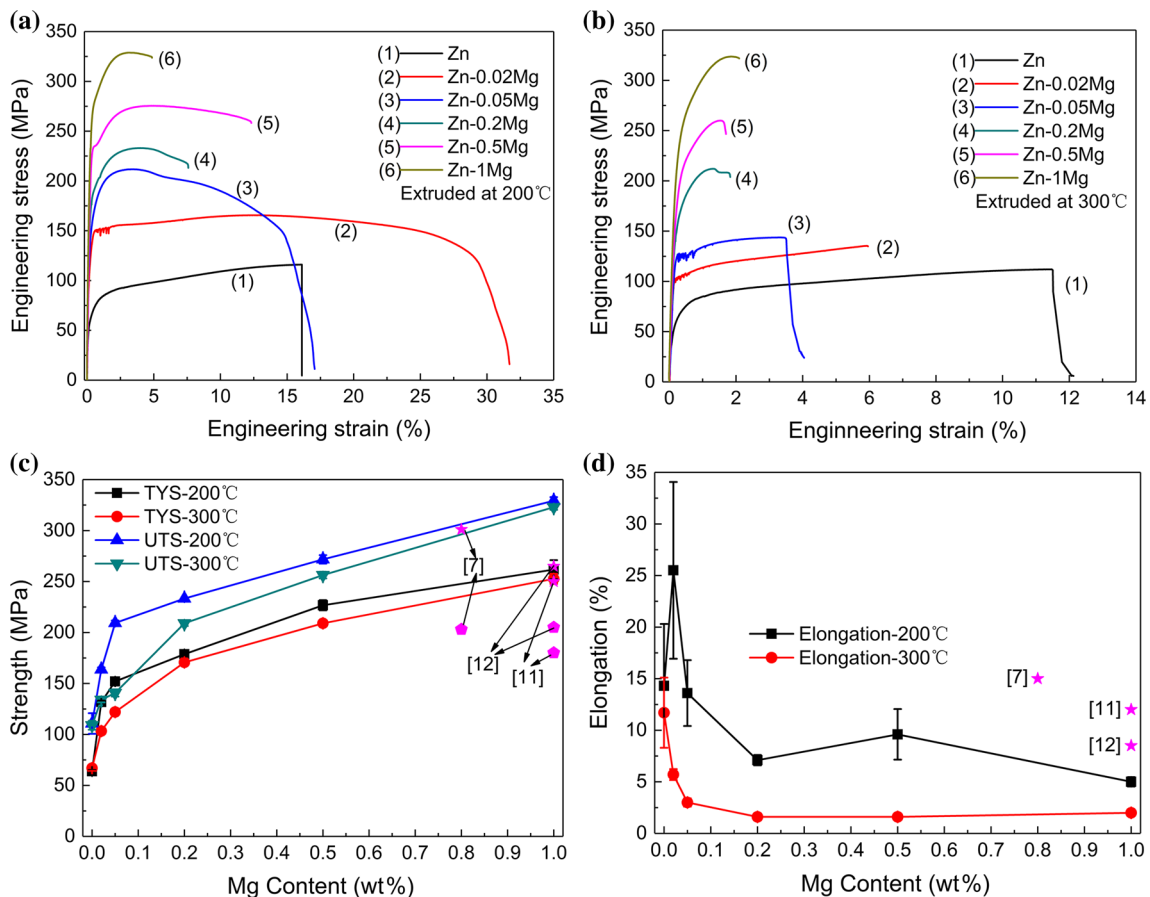


Fig. 5 Tensile stress–strain curves of the Zn–Mg binary alloys extruded at **a** 200 °C, **b** 300 °C. Tensile properties of the as-extruded Zn–Mg binary alloys: **c** strength and **d** elongation

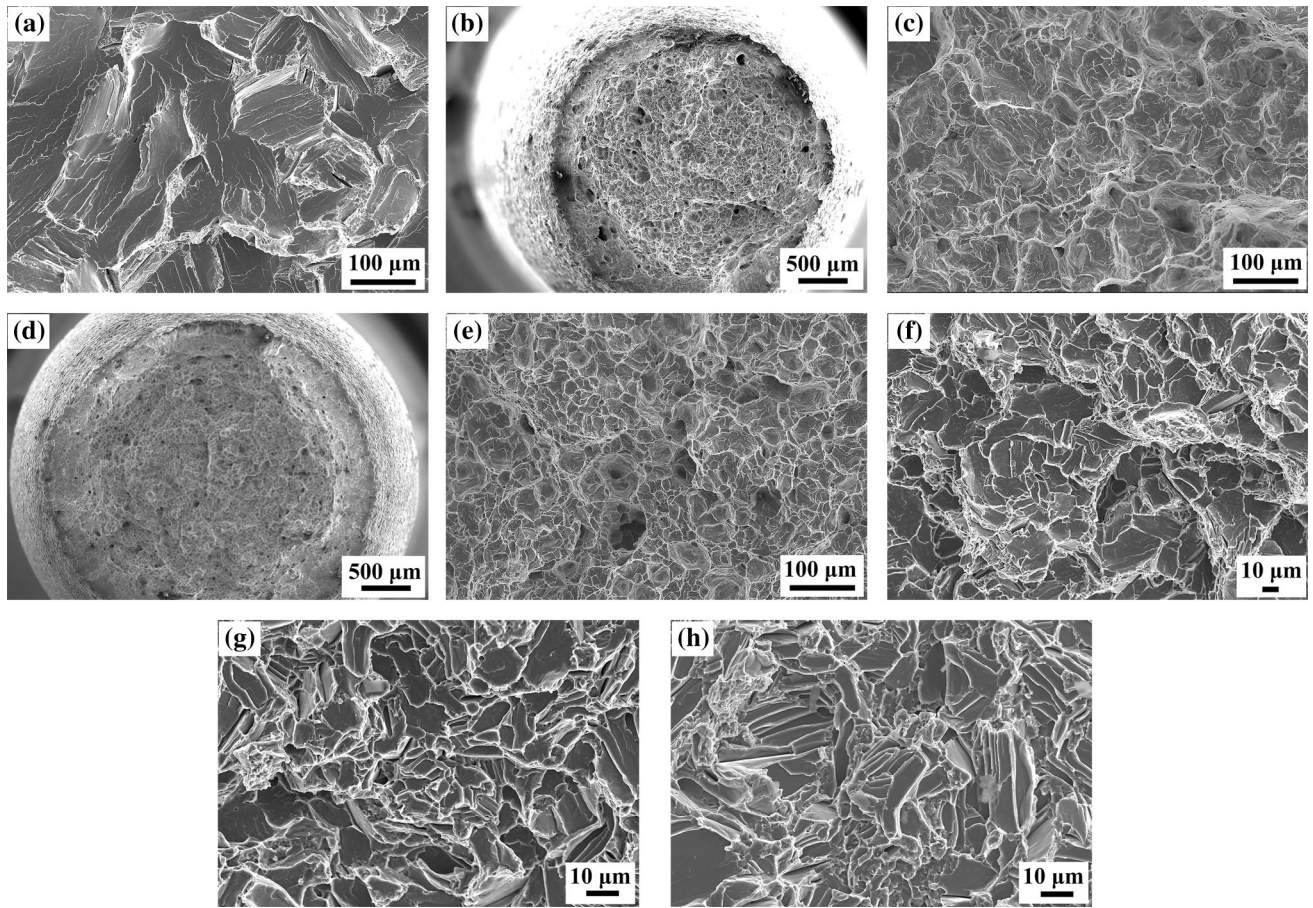


Fig. 6 Fracture morphologies of the Zn–Mg binary alloys extruded at 200 °C: **a** Zn, **b**, **c** low and high magnification of Zn–0.02Mg, **d**, **e** low and high magnification of Zn–0.05Mg, **f** Zn–0.2Mg, **g** Zn–0.5Mg, **h** Zn–1Mg

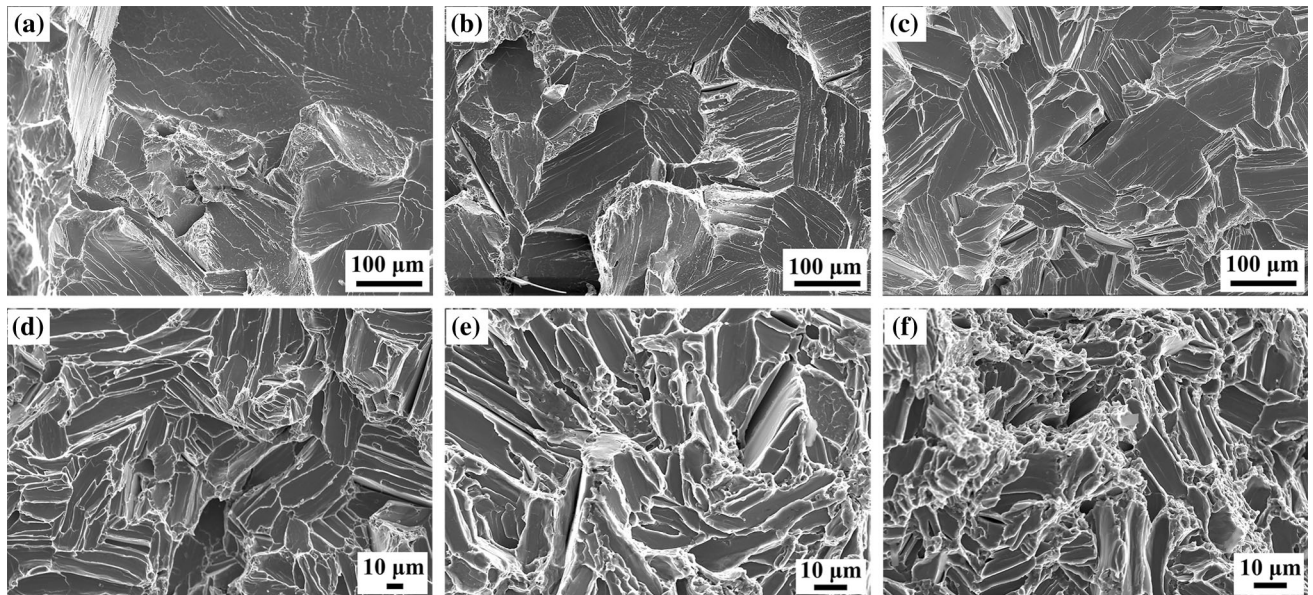


Fig. 7 Fracture morphologies of the Zn–Mg binary alloys extruded at 300 °C: **a** Zn, **b** Zn–0.02Mg, **c** Zn–0.05Mg, **d** Zn–0.2Mg, **e** Zn–0.5Mg, **f** Zn–1Mg

Table 2 Respective contributions of the strengthening mechanisms to the Zn–Mg binary alloys extruded at 200 °C

Alloys (wt%)	Zn	Zn–0.02Mg	Zn–0.05Mg	Zn–0.2Mg	Zn–0.5Mg	Zn–1Mg
d_g (μm)	112	45	24	16	9	9
d_s (μm)		0.5	0.8			
f_s		0.0037	0.0092	0.037	0.092	0.183
σ_0 (MPa)	32.3	11				
$\Delta\sigma_g$ (MPa)	20.8	86.5	118.4	145	193.3	193.3
$\Delta\sigma_s$ (MPa)	–	12.4–27.9	14.0–33.2	–	–	–
Calculated σ_y (MPa)	53.1	109.9–125.4	143.4–162.6	170.6	236.1	267.6
Tested σ_y (MPa)	64	132	152	179	227	262

Table 3 Respective contributions of the strengthening mechanisms to the Zn–Mg binary alloys extruded at 300 °C

Alloys (wt%)	Zn	Zn–0.02Mg	Zn–0.05Mg	Zn–0.2Mg	Zn–0.5Mg	Zn–1Mg
d_g (μm)	203	117	85	38	14	11
d_s (μm)		0.5	0.8			
f_s		0.0037	0.0092	0.037	0.092	0.183
σ_0 (MPa)	32.3	11				
$\Delta\sigma_g$ (MPa)	15.4	53.6	62.9	94.1	155.0	174.9
$\Delta\sigma_s$ (MPa)	–	12.4–31.6	13.7–37.7	–	–	–
Calculated σ_y (MPa)	47.7	77.0–96.2	87.6–111.6	121.6	201.3	252.5
Tested σ_y (MPa)	67	103	122	170	209	252

invalidation of Zn–Mg alloy is caused by the fracture between $\text{Mg}_2\text{Zn}_{11}$ and Zn matrix. Then, λ is simplified as 0.5. For the TYS of $\text{Mg}_2\text{Zn}_{11}$ (σ_s), typical load–displacement curve of $\text{Mg}_2\text{Zn}_{11}$ was tested by nanoindentation [26], and it showed that the hardness of $\text{Mg}_2\text{Zn}_{11}$ was 3.76 GPa; then, σ_s was calculated between 1.0 and 1.2 GPa using the method provided by Serban *et al.* [27]. Here, σ_s is taken as the average value of 1.1 GPa.

The volume fraction of the precipitate can be given as [21, 28]:

$$f_s = \frac{x\Omega^P}{x\Omega^P + (1-x)\Omega^m}, \quad (8)$$

where Ω^P and Ω^m are the average atomic volumes of the precipitate and matrix and x is the atomic fraction of the precipitate. $\text{Mg}_2\text{Zn}_{11}$ is cubic structure with $a = 0.8552$ nm, containing 39 atoms per unit cell (PDF#65-1853), while Zn is hexagonal structure with $a = 0.2665$ nm and $c = 0.4947$ nm, containing two atoms per unit cell (PDF#65-5973), so $\Omega^P = 16.0 \times 10^{-3}$ nm³ and $\Omega^m = 15.2 \times 10^{-3}$ nm³. Then, Eq. (8) simplifies as $f_s = \frac{16x}{15.2-0.8x}$.

In this work, the contribution of solid solution strengthening to TYS could be neglected due to the relative low solubility. Then, TYS of matrix (σ_M) can be expressed as $\sigma_M = \sigma_0 + \Delta\sigma_g$. Relevant parameters and calculated results of strengthening mechanism of the as-extruded Zn–

(0–1)Mg alloys are shown in Tables 2 and 3. Firstly, TYS of pure Zn was only dominated by the grain size. The grain size of Zn extruded at 200 °C was about half of that extruded at 300 °C, but both of them had similar calculated TYS which was in agreement with the experimental results. Secondly, TYS of Zn–(0.02–1)Mg alloys originates from the grain boundary strengthening and second phase strengthening. According to the calculation results, the contribution of grain boundary strengthening increases with Mg addition and accounts for more than 50%, and even it reaches 80% in the alloys extruded at 200 °C. Therefore, the grain boundary strengthening becomes the main strengthening mechanism. The contribution of second phase strengthening increases with Mg addition, even though it has different mechanisms depending on the morphology of $\text{Mg}_2\text{Zn}_{11}$. Finally, from the calculated results of the Zn–Mg alloy extruded at 200 and 300 °C, it indicates that the grain refinement primarily results in the higher TYS of the alloy extruded at 200 °C.

In addition, the mechanical properties of Zn–Mg alloys in Refs. [7, 11, 12] are shown in Fig. 5c, d and were compared with the present work. It indicated that the Zn–0.8/1Mg alloys [7, 11, 12] exhibited lower strength and higher elongation than the alloy in this work. The difference in the mechanical properties of these alloys was caused by the microstructures including grain size, kinds and size of second phase. Both of Zn–0.8Mg [7] and Zn–1Mg in the present work contained grains about 10 μm in

size. But the large-sized $\text{Mg}_2\text{Zn}_{11}$ in the present Zn–Mg alloys has more significant strengthening effect than small-sized $\text{Mg}_2\text{Zn}_{11}$ or MgZn_2 in Zn–0.8Mg [7]. And the Zn–Mg alloys with refined grains and/or second phase exhibited the improvement in elongation. The microstructure of the alloy depends on composition of alloying elements and preparation history. According to the results in the present work, the grain size strongly depends on extrusion temperature and volume fraction and size of $\text{Mg}_2\text{Zn}_{11}$, while it is known that extrusion temperature has little influence on morphology of $\text{Mg}_2\text{Zn}_{11}$. So apart from the deformation process, it is essential to control the solidification process for adjusting the morphology of $\text{Mg}_2\text{Zn}_{11}$ in the future work.

5 Conclusions

In this study, Zn–(0–1)Mg alloys were prepared by indirect extrusion with extrusion ratio of 16:1 at 200 and 300 °C, respectively. The microstructure, mechanical properties and fracture behavior were investigated, and the possible strengthening mechanisms were analyzed. The following conclusions were obtained:

In the Zn–Mg binary alloys, Mg addition induced the formation of $\text{Mg}_2\text{Zn}_{11}$, and the morphology of $\text{Mg}_2\text{Zn}_{11}$ had no difference in the alloy extruded at 200 and 300 °C. The grain refinement was achieved by increasing Mg content and/or decreasing extrusion temperature.

Both TYS and UTS of the as-extruded Zn–Mg alloys continuously increased with increasing Mg content, and they also increased at lower extrusion temperature. The Zn–Mg alloys were mainly strengthened by grain boundary strengthening and second phase strengthening, and grain boundary strengthening was in dominance.

Zn–0.02Mg and Zn–0.05Mg extruded at 200 °C exhibited a mixture of cleavage and ductile fracture mode, corresponding to higher elongation. The other alloys showed typically cleavage fracture, and the elongation decreased with increasing Mg content. Meanwhile, the alloy extruded at 200 °C showed a higher elongation than that extruded at 300 °C.

Acknowledgements This work was supported by the National Natural Science Foundation of China (Nos. 51525101 and 51371046), the Program for New Century Excellent Talents in University (No. NECT-12-0109) and the Fundamental Research Funds for the Central Universities (Nos. N130510002, N141008001).

References

- [1] R. Hansch, R.R. Mendel, *Curr. Opin. Plant Biol.* **129**, 259 (2009)
- [2] L. Rink, *Zn in Human Health* (IOS Press, Amsterdam, 2011)
- [3] D. Vojtech, J. Kubasek, J. Capek, I. Pospisilova, *Mater. Technol.* **49**, 877 (2015)
- [4] D.E. Talbot, J.D. Talbot, *Corrosion Science and Technology* (CRC Press, Boca Raton, 2007)
- [5] P.K. Bowen, J. Drelich, J. Goldman, *Adv. Mater.* **25**, 2577 (2013)
- [6] D. Vojtech, J. Kubasek, J. Šerák, P. Novák, *Acta Biomater.* **7**, 3515 (2011)
- [7] J. Kubasek, D. Vojtech, E. Jablonska, I. Pospisilova, J. Lipov, T. Ruml, *Mater. Sci. Eng., C* **58**, 24 (2016)
- [8] X.W. Liu, J.K. Sun, F.Y. Zhou, Y.H. Yang, R.C. Chang, K.J. Qiu, Z.J. Pu, L. Li, Y.F. Zheng, *Mater. Des.* **94**, 95 (2016)
- [9] X.W. Liu, J.K. Sun, Y.H. Yang, F.Y. Zhou, Z.J. Pu, L. Li, Y.F. Zheng, *Mater. Lett.* **165**, 242 (2016)
- [10] J. Kubasek, I. Pospisilova, D. Vojtech, E. Jablonska, T. Ruml, *Mater. Technol.* **48**, 623 (2014)
- [11] H. Gong, K. Wang, R. Strich, J.G. Zhou, *J. Biomed. Mater. Res. B* **103**, 1632 (2015)
- [12] H.F. Li, H.X. Xie, Y.F. Zheng, Y. Cong, F.Y. Zhou, K.J. Qiu, X. Wang, S.H. Chen, L. Huang, L. Tian, L. Qin, *Sci. Rep.* **5**, 10719 (2015)
- [13] H.F. Li, H.T. Yang, Y.F. Zheng, F.Y. Zhou, K.J. Qiu, X. Wang, *Mater. Des.* **83**, 95 (2015)
- [14] N.S. Murni, M.S. Dambatta, S.K. Yeap, G.R.A. Froemming, H. Hermawan, *Mater. Sci. Eng., C* **49**, 560 (2015)
- [15] P. Ghosh, M. Mezbahul-Islam, M. Medraj, *CALPHAD* **36**, 28 (2012)
- [16] J.H. Liu, C.X. Huang, S.D. Wu, Z.F. Zhang, *Mater. Sci. Eng., A* **409**, 117 (2008)
- [17] F.J. Humphreys, M. Hatherly, *Recrystallization and Related Annealing Phenomena*, 2nd edn. (Elsevier Science, New York, 2004)
- [18] N.G. Ross, M.R. Barnet, A.G. Beer, *Mater. Sci. Eng., A* **619**, 238 (2014)
- [19] B.Q. Shi, R.S. Chen, W. Ke, *J. Alloys Compd.* **509**, 3357 (2011)
- [20] L. Cao, R.S. Chen, E.H. Han, *J. Alloys Compd.* **472**, 234 (2009)
- [21] Y. Chen, N. Gao, G. Sha, S.P. Ringer, M.J. Starink, *Acta Mater.* **109**, 202 (2016)
- [22] Z.L. Liu, D. Qiu, F. Wang, J.A. Taylor, M.X. Zhang, *Metall. Mater. Trans. A* **47**, 830 (2016)
- [23] R. Armstrong, I. Codd, R.M. Douthwaite, N.J. Petch, *Philos. Mag.* **7**, 45 (1962)
- [24] M. Mabuchi, K. Higashi, *Acta Mater.* **44**, 4611 (1996)
- [25] J.W. Liu, X.D. Peng, M.L. Li, G.B. Wei, W.D. Xie, Y. Yang, *Mater. Sci. Eng., A* **655**, 331 (2016)
- [26] C.C. Kammerer, S. Behdad, L. Zhou, F. Betancor, M. Gonzales, B. Boesl, Y.H. Sohn, *Intermetallics* **67**, 145 (2015)
- [27] V.A. Serban, C. Codrean, M. Voda, D. Chicot, X. Decoopman, *Mater. Sci. Eng., A* **605**, 294 (2014)
- [28] A. Deschamps, A. Bigot, F.L. Vet, P. Auger, Y. Brechet, D. Blavette, *Philos. Mag. A* **81**, 2391 (2001)